Received: 7 October 2021 | Revised: 21 February 2022 | Accepted: 22 February 2022

DOI: 10.1002/wcms.1612

FOCUS ARTICLE

WIREs COMPUTATIONAL MOLECULAR SCIENCE WILEY

Power of stochastic kinetic models: From biological signaling and antibiotic activities to T cell activation and cancer initiation dynamics

Hamid Teimouri[1,2] | **Anatoly B. Kolomeisky**[1,2,3,4]

[1]Department of Chemistry, Rice University, Houston, Texas, USA

[2]Center for Theoretical Biological Physics, Rice University, Houston, Texas, USA

[3]Department of Chemical and Biomolecular Engineering, Rice University, Houston, Texas, USA

[4]Department of Physics and Astronomy, Rice University, Houston, Texas, USA

Correspondence
Anatoly B. Kolomeisky, Department of Chemistry, Rice University, Houston, TX 77005, USA.
Email: tolya@rice.edu

Funding information
National Science Foundation, Grant/Award Numbers: CHE-1953453, MCB-1941106, PHY-2019745; Welch Foundation, Grant/Award Number: C-1559

Edited by: Anna Krylov, Associate Editor

Abstract

All chemical processes exhibit two main universal features. They are stochastic because chemical reactions might happen only after random successful collisions of reacting species, and they are dynamic because the amount of reactants and products changes with time. Since biological processes rely heavily on specific chemical reactions, the stochasticity and dynamics are also crucial features for all living systems. To understand the molecular mechanisms of chemical and biological processes, it is important to develop and apply theoretical methods that fully incorporate the randomness and dynamic nature of these systems. In recent years, there have been significant advances in formulating and exploring such theoretical methods. As an illustration of such developments, in this review the recent applications of stochastic kinetic models for various biological processes are discussed. Specifically, we focus on applying these theoretical approaches to investigate the biological signaling, clearance of bacteria under antibiotics, T cells activation in the immune system, and cancer initiation dynamics. The main advantage of the presented stochastic kinetic models is that they generally can be solved analytically, allowing to clarify the underlying microscopic picture, as well as to explain the existing experimental observations and to make new testable predictions. This theoretical approach becomes a powerful tool in uncovering the molecular mechanisms of complex natural phenomena.

This article is categorized under:

Molecular and Statistical Mechanics > Free Energy Methods
Structure and Mechanism > Computational Biochemistry and Biophysics
Theoretical and Physical Chemistry > Statistical Mechanics

KEYWORDS

bacterial clearance, biological signaling, cancer initiation, dynamic processes, stochastic models

1 | INTRODUCTION

Chemical reactions are unique dynamic phenomena that occur when several original types of molecules, called reactants, transform into other types of molecules, called products. This is the result of complex molecular interactions that typically take place after reactant molecules are able to collide with each other, leading to breaking old and creating new chemical bonds. The crucial properties of chemical reactions are their stochastic nature and complex dynamic behavior.[1] Due to random collision of reactants, typical chemical reactions have broad distributions of time scales that characterize the completion of these processes. The composition of the system where chemical reactions are taking place also evolves with time. Various chemical kinetic methods, both experimental and theoretical, have been developed to comprehensively analyze temporal and spatial evolution of chemical reactions, providing important insights on the underlying molecular mechanisms.[1]

Chemical reactions are obviously critically important for all biological systems.[2] Traditionally, deterministic macroscopic kinetic models have been utilized to describe the chemical aspects of most cellular processes.[3] In this approach, it is assumed that components of the system are always well mixed and easily available, and the temporal evolution of concentrations of participating molecules can be obtained by solving corresponding differential equations that describe the temporal evolution of every type of species. However, there are multiple limitations for the application of deterministic macroscopic kinetic models for understanding the processes in living systems. First, in biological systems the copy numbers of participating molecular species can be very low, which, in turn, can give rise to significant fluctuations in concentrations and a wide spectrum of relevant time scales.[3–5] In addition, the deterministic models typically describe only the average stationary properties of the system, and they fail to capture a complex transient behavior with transitions between different states.[3,5] Furthermore, the importance of mesoscopic stochastic dynamic models have been especially realized recently with the developments in single-molecule experimental techniques that allowed to probe complex biological systems with unprecedented spatial and temporal resolutions.[6,7] Clearly, to understand better the microscopic picture of cellular processes, one needs to utilize theoretical frameworks that comprehensively accounts for both stochastic and dynamic effects.

In recent years, a significant progress has been achieved in developing various theoretical methods that better reflect the random dynamic nature of biological processes.[5–8] The main idea of such stochastic kinetic models (although other labels for such models have been also used) is that the investigated processes in the underlying biological system can be viewed as a set of continuous-time transitions between discrete states. These discrete states, depending on the context of the problem, might reflect different spatial positions, different number of cells, or different molecular conformations. The transitions between these states are random and specified by the local dynamic rules that depend on molecular interactions and energy changes in the system. In this review, several stochastic kinetic models and their applications for various biological phenomena are presented. We specifically focus on microscopic mechanisms of morphogen gradients formation, stochastic clearance of bacteria by antibiotics, T cell activation in the immune system, and cancer initiation dynamics. The main advantage of this approach is the ability to obtain explicit analytic descriptions for most relevant properties of these systems, allowing for better understanding of underlying molecular mechanisms. Our goal is not only to illustrate the method of stochastic kinetic models but also to show that this approach is a powerful tool in studying complex chemical and biological processes.

2 | MORPHOGEN GRADIENT FORMATION

Development of complex multicellular organisms from a single embryonic cell remains one of the most fascinating and still not fully understood fundamental biological processes.[9–11] It is known that at some time the dividing embryo cells start to differentiate, producing complex patterns that eventually transform into specific tissues and organs. A critical role of several classes of protein molecules, known as *morphogens*, is now well established.[9–12] After intensive experimental investigations,[13–15] the following picture emerged about the activities of these biological signaling molecules.[16] At some stage of the development process, one or several embryo cells start to produce morphogens into the medium in which other embryo cells coexist. This is a symmetry-breaking event that allows to eventually distinguish different parts of the growing embryo system. As the sign of this symmetry breaking, the signaling molecules via different distribution mechanisms establish a non-uniform concentration profile as schematically shown in Figure 1. Different genes are being then activated at the underlying embryo cells depending on the local concentration of morphogens: see Figure 1. This leads to the final pattern formation and full differentiation of tissues and organs in the developed organisms.

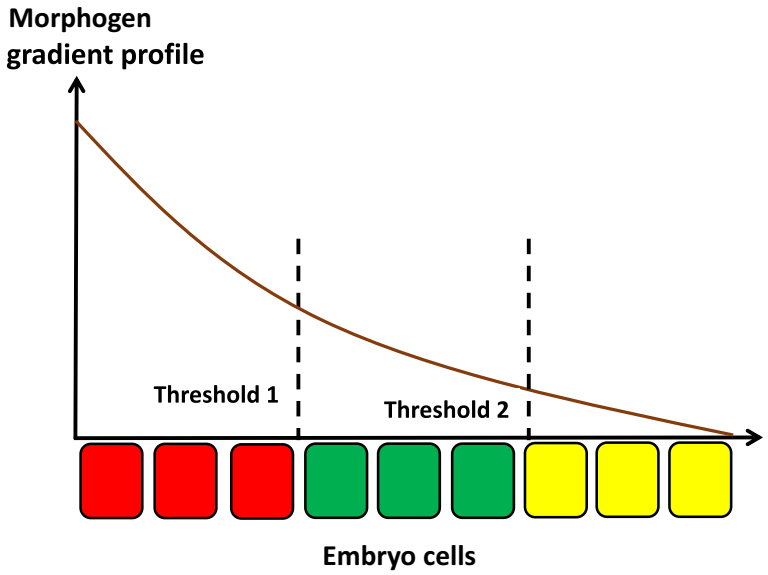

FIGURE 1 A schematic cartoon of how the non-uniform concentration profile of morphogen molecules leads to different activation of underlying embryo molecules. For the region before threshold 1, cells will activate only a "red" gene; for the region between threshold 1 and threshold 2, cells will activate only a "green" gene; and for the region after threshold 2, cells will activate only a "yellow" gene

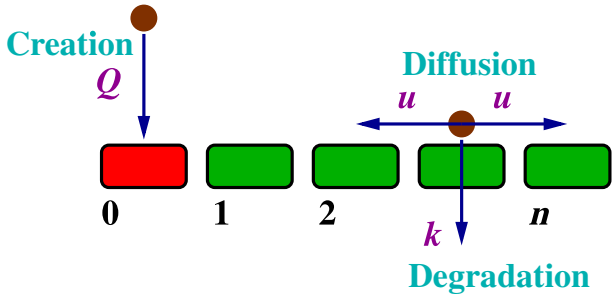

FIGURE 2 A scheme for the simplest one-dimensional discrete-state stochastic model for the formation of morphogen gradient. Signaling molecules are produced at the site 0 (shown in red) with a rate Q. Morphogens might diffuse along the lattice to the neighboring sites with a rate u, or they might be degraded with a rate k

This picture of how the morphogens are operating raised several important questions: what are the microscopic mechanisms of the formation of non-uniform concentration profiles (also called *morphogen gradients*) and how fast they can be established? Various theoretical ideas to answer these questions have been proposed.[13–23] It is widely believed that the morphogen gradients are the result of complex action of chemical and physical forces.[13–15,24,25] The signaling molecules might associate to cell receptors and be effectively removed from the system by initiating the biochemical cascades inside the embryo cells that activate specific genes, but they can also diffuse in the medium. These arguments led to the development of the simplest, but still the most widely utilized, theoretical approach, which is known as a *synthesis–diffusion–degradation* (SDD) model.[13–15,24,25] It is also important to note that the morphogen molecules are removed from the system at specific sites that are spatially separated from each other (cell receptors at different embryo cells). This indicates that the formation of morphogen gradient must be considered as a discrete biochemical process. For this reason, we present here a discrete-state stochastic model that investigates the molecular origin of the fast and robust development of morphogen gradients.[17,26] Our aim here is to show how the explicit analysis of such theoretical model clarifies many aspects of this complex biological phenomenon.

Let us consider a model illustrated in Figure 2. Given the fact that most experimental studies on the morphogen gradient formation explore the *Drosophila* where embryo cells are arranged in a quasi-one-dimensional order,[13,24] the proposed theoretical approach views the system a linear semi-infinite chain of lattice sites $n \geq 0$. Each site corresponds to a different embryo cell. The model assumes that morphogens are created at the origin ($n = 0$) with a rate Q. Then the

signaling molecules can diffuse along the lattice with a rate u, while they can also be degraded (removed from the system) at any site with a rate k: see Figure 1.

Because the morphogens are independent of each other, it is convenient to adopt a single-molecule view of the processes and follow the changes in the particle occupations. For this purpose, one can introduce a function $P_n(t)$ which is defined as the probability density to find the morphogen molecule at the site n at time t. The evolution of this probability is governed by the following master equations,

$$\frac{dP_0(t)}{dt} = Q + uP_1(t) - (u+k)P_0(t), \tag{1}$$

for $n = 0$; and

$$\frac{dP_n(t)}{dt} = u[P_{n-1}(t) + P_{n+1}(t)] - (2u+k)P_n(t), \tag{2}$$

for $n > 0$. These expressions simply reflect the conservation of the probability of finding the morphogen at the given location. At large times, when $\frac{dP_n(t)}{dt} = 0$, the system reaches the steady-state conditions, and these equations can be easily solved,[17,27] producing an exponentially decaying concentration profile,

$$P_n^{(s)} = \frac{2Qx^n}{k + \sqrt{k^2 + 4uk}}, \tag{3}$$

with

$$x = \frac{2u + k - \sqrt{k^2 + 4uk}}{2u}. \tag{4}$$

These predictions qualitatively agree with multiple observations of morphogen gradients in different biological systems.[28–31]

In Figure 3a, we present typical concentration profiles of the signaling molecules as predicted by this theoretical model. One can see that the concentration of signaling molecules decreases for larger degradation rates, and the stationary morphogen gradient has a decay length

$$\lambda = -\frac{1}{\ln x}, \tag{5}$$

which in the limit of fast diffusion ($u \gg k$), also known as the continuum limit, reduces to a well-known relation $\lambda \simeq \sqrt{u/k}$.[17,32] This result emphasizes that the characteristic length scales created by the nonuniform concentration profiles of signaling molecules are due to the balance between the diffusion and the degradation processes. It also suggests how the thresholds in the developmental pattern formation might be specifically regulated at the cellular lever, providing an important insight on the mechanisms of these complex biological processes.

This theoretical approach is also able to evaluate the dynamics of approaching to the stationary properties and to resolve the apparent paradox of slow morphogen diffusion and fast formation of the morphogen gradient.[16,17,28,33] This paradox is based on the following observations. Experiments on measuring the diffusion of bicoid morphogen proteins in *Drosophila* embryo (size $L \sim 400$ μm) determined that signaling molecules diffuse not so fast with $D \sim 1$ μm^2/s. One could argue then that if the morphogen molecules are produced at one end of the embryo, to reach the other end to establish the gradient would need a time of at least $\tau \simeq L^2/D \sim 3000$ min, while the experiments clearly observe that the morphogen gradient was created in <100 min,[28] that is, almost two orders of magnitude faster.

These controversial observations were explained later by applying the method developed by Berezhkovskii et al.[22,32,34] According to this approach, the time scales to establish the morphogen gradients are given by the local relaxation times to reach the stationary state from the originally empty system (before the morphogen production

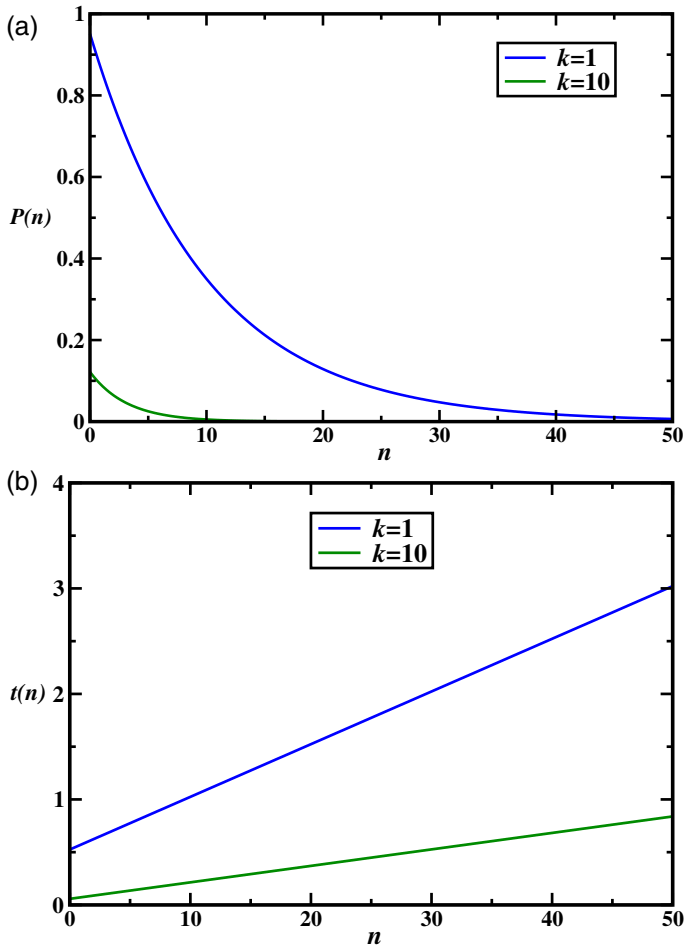

FIGURE 3 (a) Stationary-state density profiles of morphogen molecules as a function of the distance from the production site for different degradation rates. (b) Relaxation times to reach the stationary-state morphogen gradients as a function of the distance from the production site for different degradation rates. The following parameters were used in calculations: $Q = 10\ \mathrm{s}^{-1}$ and $u = 100\ \mathrm{s}^{-1}$

starts). These times are labeled as *local accumulation times* (LAT), and they are closely related to so-called local relaxation functions,[32]

$$R(n;t) = \frac{P(n;t) - P^{(s)}(n)}{P(n;t=0) - P^{(s)}(n)} = 1 - \frac{P(n;t)}{P^{(s)}(n)}. \tag{6}$$

One could easily understand the physical meaning of these functions. They can be viewed as the relative distance of the system from the stationary state at the given location. At $t = 0$, such distance is one ($R = 1$), and it approaches zero at $t \to \infty$ when the steady-state at the given location is already reached. One could also see that $\left(-\frac{\partial R(n,t)}{\partial t}\right)$ is the probability density to reach the stationary state at the site n at time t. Then using the Laplace transform of the function, $\widetilde{R}(n,s) = \int_0^\infty R(n;t)e^{-st}dt$, it can be shown that the LAT are given by

$$t(n) = -\int_0^\infty t\frac{\partial R(n;t)}{\partial t}dt = \int_0^\infty R(n,t)dt = \widetilde{R}(n;s=0). \tag{7}$$

From this relation, the explicit expression for the local accumulation times in the discrete-state stochastic from Figure 2 can be found,[17]

$$t(n) = \frac{1}{\sqrt{k^2+4uk}}\left[\frac{2u+k+\sqrt{k^2+4uk}}{k+\sqrt{k^2+4uk}}+n\right], \tag{8}$$

which in the continuum limit ($u \gg k$) produces

$$t(n) = \frac{1}{2k}\left(1+\frac{n}{\lambda}\right). \tag{9}$$

The results for the relaxation times to reach the steady state are presented in Figure 3b. One can see that they depend linearly on the distance from the source, and increasing the degradation rate accelerates reaching the stationary state. This observation can be easily understood by comparing the corresponding morphogen gradients (Figure 3a). For larger degradation rates, the stationary concentration of signaling molecules is lower, and then it can be reached faster from the originally empty system.

The model was successfully applied for analyzing the morphogen gradient formation of bicoid proteins in fruit fly embryos.[19,28,35] Experimental measurements suggest that the decay length of the concentration profile of signaling molecules is $\lambda \simeq 60$ μm, which allowed researchers to estimate the relaxation to reach the stationary state at the furthest end of the embryo ($L \simeq 400$ μm) using the simplest SDD model (Equation (8)) as ∼200 min. This should be compared with ∼100 min observed in experiments. Considering more realistic models of longer spatially localized exponentially distributed source regions,[16,26] however, brings the theoretical estimate much closer to experimental observations, suggesting that this theoretical approach probably captures the main features of the morphogen gradient formation.

But the most important result of the discrete-state stochastic model is the ability to explain the faster than expected formation of the morphogen gradients.[16,17] One can see it in Figure 3b that shows the linear dependence of LAT ($t(n) \sim n$), in contrast to expected quadratic scaling for the relevant times scales. The linear scaling is the reason for quickly reaching the stationary state in the system. From microscopic point of view, this acceleration can be explained by noticing the important role of the removal of the morphogen molecules from the system. At each embryo cell, there is a non-zero probability for signaling molecules to be degraded. Only the fastest morphogen particles will survive, effectively leading to the acceleration of the whole process of the morphogen gradient formation. This might be also viewed as an example of selection effect or selection bias, which is a well-known concept in statistics. Another way to look into this phenomenon is to associate the degradation with en effective potential $U_{\text{eff}}(n)$ that effectively drives the morphogen particles away from the source. At the molecular level, each morphogen particle has equal probability to go in both directions (see Figure 1), but more signaling molecules are removed further away from the source (larger n) because they came to the system earlier at the site $n = 0$. This leads to the creation of the concentration gradient that moves particles fast away from the production source. This potential can estimated from the steady-state concentration profile,[16,17]

$$U_{\text{eff}}(n) \simeq k_B T \ln P_n^s = n \ln x = -\frac{n}{\lambda}. \tag{10}$$

This strong linear potential corresponds to a constant effective force at every site,

$$F_{\text{eff}} = -\frac{\partial U_{\text{eff}}(n)}{\partial n} = \frac{1}{\lambda}, \tag{11}$$

that displaces the morphogen particles away from the production region. This picture of the effective potential due to the degradation processes also explains the linear dependence of LAT on the distance from the source (see Figure 3b). This is because the process of the formation of the morphogen gradient is a driven process with the expected linear scaling as a function of the distance. It is not the unbiased diffusion with quadratic scaling, as one would naively expect. These arguments fully explain the fast formation of the morphogen gradients and resolve the paradox of slow diffusion.

A discrete-state stochastic SDD model provides a comprehensive description of microscopic process of the formation of morphogen gradients. It argues that the non-uniform concentration profiles, required in order to properly transfer the genetic information, are created as a balance between the molecular diffusion of morphogen particles and their degradation. However, the removal of signaling due to degradation is critically important for accelerating the dynamics of

the formation of stationary profiles. This theoretical approach is able to successfully explain the existing experimental observations. Because of the explicit nature of these discrete-state stochastic models, they seem to be a very useful approach to quantitatively investigate the complex mechanisms of biological development processes.

3 | STOCHASTIC CLEARANCE OF BACTERIA

Another example of successful application of the stochastic kinetic approach is theoretical investigations of bacterial clearance by antibiotics or antimicrobial peptides.[36,37] It is well recognized that the rise of pathogenic bacteria that are resistant to antibiotics is one of the most critical global health issues. This is related with the fact that current antibiotic treatments cannot fully eradicate the bacteria that are susceptible to them, allowing the remaining microbes to develop the resistance to the medical drugs.[38,39] Current experimental and theoretical studies of bacterial clearance by antibiotics concentrate mostly on the removal of large quantities of microbes, applying for these purposes a deterministic analysis.[40–42] The central quantity in this deterministic framework is a minimal inhibitory concentration (MIC), which is defined as a minimal drug concentration that fully inhibits bacterial growth.[42–44] It is widely assumed that MIC is the critical antibiotic concentration above which the bacteria will be always eliminated, but for the lower concentrations the infection will not be stopped.

However, there is an increasing number of experimental evidences suggesting that the deterministic approach fails to properly describe the clearance of small bacterial populations where stochastic effects are dominant.[36] This is especially important for the systems where a small number of surviving bacteria can easily restart the infection, as happens, for example, for *Salmonella* and *Shigella* bacteria.[45–47] In addition, the surviving bacterial cells can develop the antibiotic resistance faster, and only the full bacterial eradication will stop the infection.[48–52] Recent experimental advances allowed researchers to quantify the dynamics of antibiotic-induced removal of small populations of bacteria,[53] providing the ground for the development of corresponding theoretical methods.[36,39,53] Let us present a specific discrete-state model of bacterial clearance that illustrates the power of the stochastic kinetic approach in uncovering the microscopic mechanisms of this complex biological phenomenon.

To describe the bacterial clearance dynamics, a simple discrete-state stochastic model, as presented in Figure 4a, is considered.[36] It describes an organism with some number of bacterial cells inside which is also simultaneously treated by the constant concentration of antibiotics to remove the infection. There are $N + 1$ possible states in the system. The states labeled as n correspond to the situation with exactly n bacteria cells inside the host organism. The state $n = 0$ describes the system where all bacterial cells are eradicated, which is the final goal of the application of antibiotics. It is labeled as an *extinction state* (see Figure 4a). The state $n = N$ describes the situation when the overall system goes into another metabolic state. It could be the situation when bacteria damage the cell membrane and normal biochemical processes inside the host organism, which might even lead to the death. It could also trigger a strong immune response from the host organism. In any case, the dynamics in the system changes dramatically, and we label this state as a *fixation state* (see Figure 4a).

While the bacterial cell growth and death involve multiple complicated physical and chemical processes, to simplify the analysis, it is assumed that dynamics in the system can be described by only two effective stochastic processes.[36] The bacterial cells can grow with a rate λ or they can dye with a rate ϕ. This means that transitions in the system follow the sequence of the states presented in Figure 4a. From the state n, the system can move to the state $n + 1$ with the overall rate $n\lambda$, increasing the level of bacterial infection. It can also move to the state $n - 1$ with the overall rate $n\phi$, decreasing the level of bacterial infection. Additionally, it is assumed that the bacterial cell growth rate is independent of antibiotic concentration, while the cell death rate is a function of the antibiotic concentration.[54] In the simplest case, the linear dependence is assumed but experimental measurements suggest more complex relations between the death rate and the concentration of antibiotics.[54]

Analysis of the system suggests that there are only two outcomes in the bacterial clearance process. The infection is fully removed when the system reaches the state 0, or the antibiotic treatment fails when the system reaches the state N. These arguments indicate that first arrivals to these absorbing final states specify the critical properties of the bacterial clearance. Then it is convenient to utilize a first-passage theoretical method[55,56] to analyze the dynamics in the system.[36] For this purpose, one can introduce a function $F_n(t)$, which is defined as a probability density function to clear the system from infection at time t if the initial number of bacterial cells in the host organism (known as an *inoculum* size) is equal to n ($1 \leq n \leq N - 1$). The temporal evolution of these probability functions are given by the so-called backward master equations,[36,55,56]

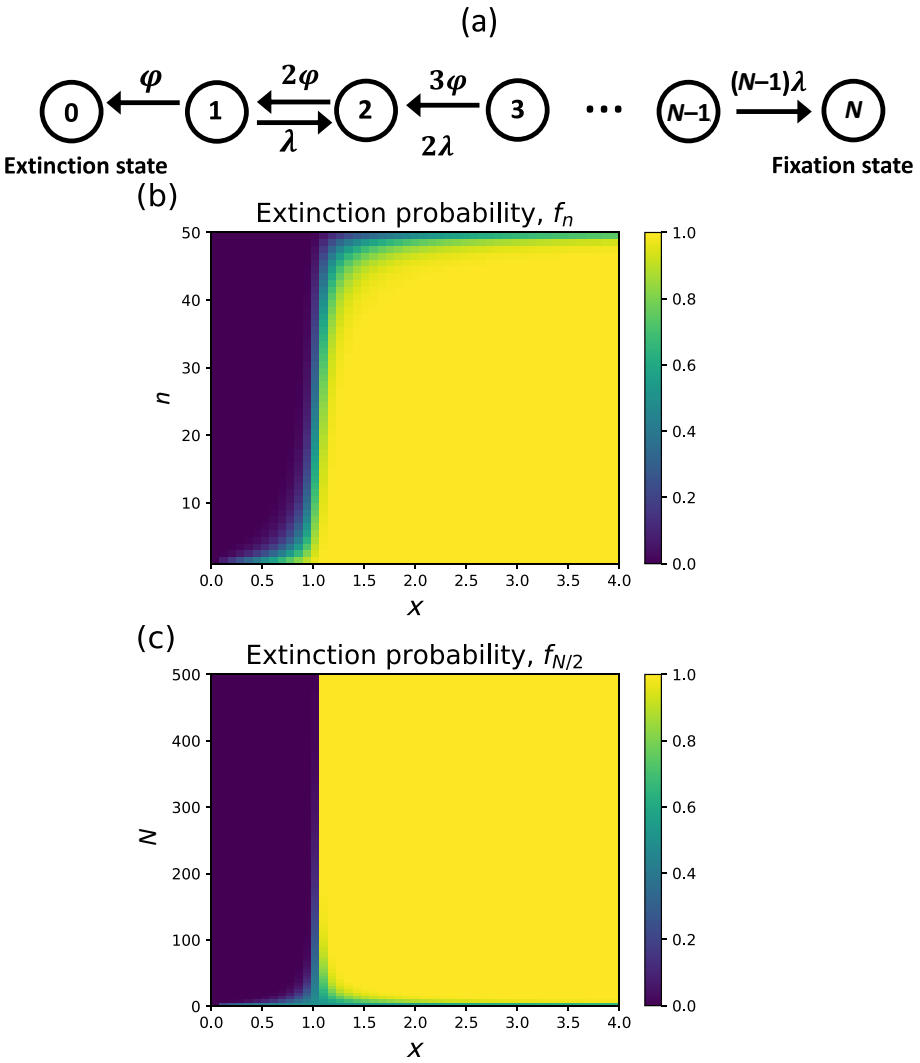

FIGURE 4 (a) Schematic view of the stochastic model for the clearance of bacteria. Each state n ($n = 0, 1, ..., N$) represents a bacterial population with n cells. The states 0 and N correspond to the bacterial eradication (no cells in the system), and the fixation, respectively. From each state n, the bacterial population can change to the state $n + 1$ (growth) with a total rate $n\lambda$, or it can jump to the state $n - 1$ (shrinking) with a total rate $n\phi$. We define normalized death rate, x as the ratio of death rate and growth rate, $x = \phi/\lambda$. Analytical calculations of extinction probabilities (b) over $n - x$ parameter space for $N = 50$; (c) for a specific mid-size inoculum ($n = N/2$) over $N - x$ parameter space. The figures are reproduced with permission from Ref. [36]

$$\frac{dF_n(t)}{dt} = n\phi F_{n-1}(t) + n\lambda F_{n+1}(t) - n(\lambda+\phi)F_n(t). \tag{12}$$

These equations describe the conservation of the probability density.

It is important to discuss the physical meaning of the first-passage probability density function $F_n(t)$.[56] Imagine that we start from the state n at $t = 0$, and the trajectories of all possible modifications in the system as a function of time are followed. These "measurements" are repeated many times starting from the same initial site n. To understand the dynamics of bacterial clearance, we record only those trajectories that come to the extinction state or to the fixation state in the time interval between t and $t + dt$. Such events are considered as successful events. Then the fraction of these successful events that end up at the state $n = 0$ gives the probability density function $F_n(t)$. In other words, $F_n(t)$ describes the conditional first-passage time distribution to reach the extinction state.

The distributions of extinction times $F_n(t)$ can be obtained analytically, providing a convenient path to analyze the dynamics of bacterial clearance for this model.[36] More specifically, two quantities are the most relevant for this analysis.[36] One of them is an extinction probability f_n, which is defined as the overall probability for the bacterial population

with the inoculum size n to completely eradicate the infection. The second is a mean extinction time T_n, which is defined as the mean first-passage time to reach the extinction state ($n = 0$) starting initially from the inoculum size n.

It could be shown that the extinction probability is given by the following simple expression,[36]

$$f_n = \frac{x^N - x^n}{x^N - 1}, \tag{13}$$

where a new important parameter $x = \phi/\lambda$ can be viewed as an effective death rate for the bacterial population normalized over the growth rate. For $x > 1$, the bacterial clearance due to large antibiotic concentrations dominates over the cell growth, while for $x < 1$ (low antibiotic concentrations) the situation reverses. The case $x = 1$ corresponds to the antibiotic concentration when the bacterial clearance is balanced by the cell growth, and it can be viewed as the analog of MIC from the deterministic analysis of this process.

Theoretical predictions for the extinction probabilities are presented in Figure 4b,c. It shows the dependence of the probability to clear the bacterial infection on the initial size of bacterial population n and on the effective death rate x. When the bacterial growth rate is equal to the death rate ($x = 1$), the extinction probability has a very simple expression,[36]

$$f_n(x=1) = \frac{N-n}{N}. \tag{14}$$

In this case, the probability of bacterial clearance is given by the relative distance from the initial state n to the fixation state N. In other words, the smaller the initial number of bacterial cells in the system, the more probable is to clear them from the host.

For sub-MIC conditions ($x < 1$), the bacterial growth rate is faster than the death rate, and, as expected, it is harder to eliminate the infection. The extinction probability in this case (making a realistic assumption that $N \gg 1$) behaves like

$$f_n \simeq x^n. \tag{15}$$

This indicates that the extinction probability is a decreasing function of the inoculum size n. But, importantly, even for such sub-MIC conditions the probability of extinction is not equal to zero as postulated by the deterministic approach. This is a clear sign of stochastic effects in the bacterial clearance. Similar stochastic effects can be exhibited in the case of large antibiotic concentrations (above MIC, $x > 1$), when for the realistic case of $N \to \infty$ the extinction probability is given by

$$f_n \simeq 1 - x^{n-N}. \tag{16}$$

It approaches to one but never equals to one as assumed in the deterministic approach.

A better indication of the dynamics of bacterial eradication can be obtained by analyzing the mean extinction times. These are the average times before the infection can be completely cleared from the host organism. They are critically important for development of new medical strategies as well as to quantify the bacterial tolerance to already existing antibiotics.[57] The idea here is that the longer bacteria can survive at given conditions, the sooner it will develop a resistance to the drug. Theoretical analysis of the discrete-state stochastic model of bacterial clearance provides an explicit expression for the mean extinction times,[36]

$$T_n = \frac{1}{\lambda(x^N - x^n)(x-1)} \left[\frac{1-x^n}{1-x^N} \sum_{k=1}^{N-1} \frac{\left(x^N - x^k\right)\left(x^{N-k} - 1\right)}{k} - \sum_{k=1}^{n-1} \frac{\left(x^N - x^k\right)\left(x^{n-k} - 1\right)}{k} \right]. \tag{17}$$

For conditions corresponding to MIC ($x = 1$), this result modifies into

$$T_n = \frac{1}{\lambda(N-n)} \left[\frac{n}{N} \sum_{k=1}^{N-1} \frac{(N-k)^2}{k} - \sum_{k=1}^{n-1} \frac{(N-k)(n-k)}{k} \right]. \tag{18}$$

For large antibiotic concentrations ($x > 1$ and assuming $N \to \infty$) the mean extinction times are given by,

$$T_n = \frac{1}{\lambda}\left[\frac{x^n - 1}{x-1}\ln\left(\frac{x}{x-1}\right) - \sum_{k=1}^{n-1}\left(\frac{1}{k}\sum_{j=0}^{n-k-1} x^j\right)\right]. \tag{19}$$

At the same time, for sub-MIC conditions ($x < 1$), it can be shown that

$$T_n \simeq \frac{1}{\lambda}\left[\frac{1}{n} + \frac{x}{n+1} + \ldots\right]. \tag{20}$$

The results of analytical calculations for the mean extinction times at different conditions are presented in Figure 5. The mean extinction time is the increasing function of the inoculum size, as illustrated in Figure 5a. This result is expected because for larger initial bacterial populations it takes longer to completely remove all microbes. More unexpected behavior is found for the mean extinction times as the function of different antibiotic concentrations: see Figure 5b. It is found that $T(n)$ is a non-monotonic function of the parameter x, and the slowest dynamics is observed for the MIC conditions ($x = 1$). It is easy to understand why for large antibiotic concentrations ($x > 1$) the mean extinction time quickly decreases. This is because for larger x the tendency to eradicate the infection is stronger. However, the fact that the mean extinction times are also fast for low antibiotic concentrations ($x < 1$) is rather very surprising since at these conditions the tendency to grow overcomes the death rates. To understand this observation, one should recall again the definition of the mean extinction time. It is a *conditional* mean first-passage time to reach the state $n = 0$ starting from the state n. The condition is that the time is estimated only for those trajectories that lead to the successful eradication. Such events are rare for $x < 1$, but they must be fast in order for the bias to growth transitions not to stop them. In other words, even for sub-MIC conditions, the bacterial clearance can be fast, but the probability of such events is low. However, this scenario is typically not feasible in real biological systems.

One could also explain the slowest clearance dynamics for $x = 1$. Transitions in the system can be viewed as a random walk along the lattice of discrete state shown in Figure 4a. Then, the MIC conditions describe an unbiased random walk ($\phi = \lambda$), which is known to evolve much slower than the biased random walks for $x < 1$ and $x > 1$. These arguments suggest a new more practical reinterpretation of the MIC. It is the antibiotic concentration at which the mean extinction times are maximal (eventually even diverging for very large bacterial populations $N \to \infty$).

The discrete-state stochastic model of bacterial clearance presents a comprehensive view on the eradication of infection by antibiotics. It provides a more physically reasonable definition of the MIC, which deviates from the binary picture adopted by the deterministic framework. It argues that, when the bacterial populations are not large and stochastic

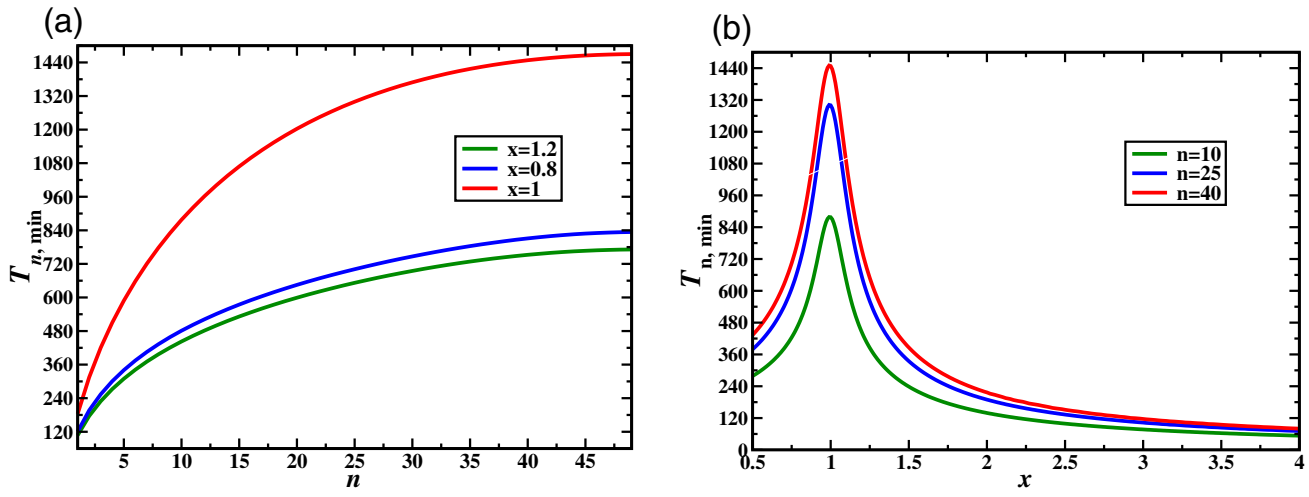

FIGURE 5 Analytical calculations for the mean extinction times (in min): (a) as a function of the inoculum size for three different values of x; and (b) as a function of the parameter x for different inoculum sizes ($n = 10$, 25, and 40). In all calculations $N = 50$ and $\lambda = 1/60$ min^{-1} were utilized. The figures are reproduced with permission from Ref. [36]

effects become relevant, the probability of clearance might be larger than zero even for the sub-MIC conditions, or less than one even for the antibiotic concentrations larger than MIC. In addition, this theoretical approach suggests and explains why the eradication dynamics has a complex non-monotonic dependence on the antibiotic concentrations. Furthermore, it gives a practical advice on how to apply the antibiotics at the conditions far away from MIC in order to avoid the expected slowing down in the bacterial clearance dynamics.

4 | KINETIC PROOFREADING MODEL OF T CELL ACTIVATION

Stochastic kinetic models also turned out to be very useful in studying the mechanisms of activation of the adaptive immune systems, and specifically for understanding the *T cells* signaling.[58–68] T cells are important components of the immune system of healthy organisms that are critical for detecting and responding to various diseases.[59,69] It is believed that they become activated after T cell receptors (TCR) bind to a specific protein assembly, known as peptide major histocompatibility complex (pMHC) that is found on the surface of antigen-presenting cells. This situation is schematically shown in Figure 6a.

How T cells are responding to the invasion of foreign pathogens is quite complex.[70–72] They must simultaneously exhibit high degrees of sensitivity, specificity, and the activation must happen fast. This is because the T cells must react to very few foreign peptides in the medium full of self-peptides that are chemically very similar. The reaction must be rapid in order for the infection not to affect the host organism. The unique mechanisms of T cells activation stimulated multiple theoretical and experimental investigations that clarified some aspects of their activities.[58,60–65,67,68,73–76] To illustrate the power of stochastic kinetic models, we present here a simple discrete-state model for T cell signaling.[76] It quantitatively describes all relevant properties of the activation process, allowing to explain the unique sensitivity, specificity, and speed of the immune T cells.

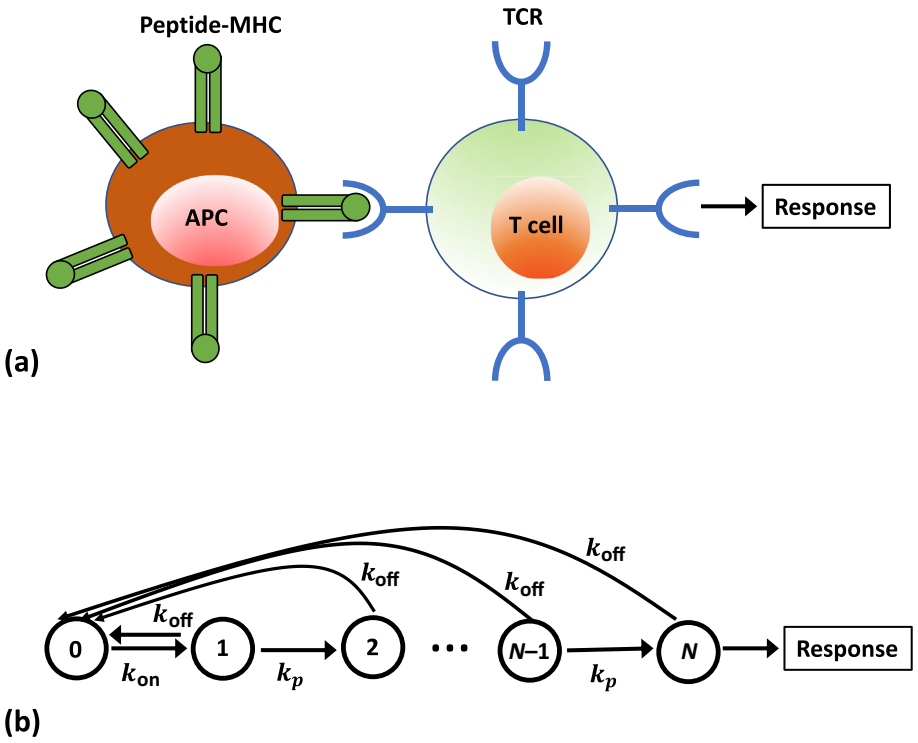

FIGURE 6 (a) A schematic description of activation of a T cell during the immune response. The T cell binds to a corresponding TCR receptor located the antigen presenting cell. If the foreign peptide is identified, the response is activated. (b) A schematic view of the simplest kinetic proofreading model for the antigen discrimination. Each state n ($1 \le n \le N$) corresponds to a complex between TCR and pMHC with a different degree of phosphorylation. State $n = 0$ describes the unbound TCR and pMHC species. The immune response is activated when the system reaches the state $n = N$ and the stationary concentration for this state is achieved. The figures are reproduced with permission from Ref. [76]

Although the molecular details of how T cells become activated are still not fully understood, the dominating view in the field relies on the idea of *kinetic proofreading* (KPR).[59,77,78] According to this approach, the activation is a process that starts after the binding of TCR to the corresponding pMHC, which is followed by several consecutive phosphorylation transformations until the final state that can activate the immune response is achieved. However, from any intermediate state the TCR can relax without reaching the final state by simply dissociating from pMHC. This allows T cells to correct the errors due to binding the wrong peptide complexes. This is critically important because the inappropriate activation of T cells might lead to serious allergic and autoimmune diseases.[59] The KPR mechanisms of controlling the activation of T cells are supported by various experimental observations.[74,75]

Theoretical model of T cells activation, presented in Figure 6b, is the simplest KPR model that can be explored for understanding the underlying processes of the immune system activation.[76] It postulates that there are N ($n = 1, 2, ..., N$) discrete states of association between TCR and pMHC that differ by the level of phosphorylation. The discrete parameter n measures the degree of phosphorylation of TCR-pMHC complex. In addition, the state $n = 0$ describes the situation when the ligand and receptor are not bound to each other. It is assumed that the final phosphorylated state $n = N$ is capable to start the activation of the immune response by triggering the corresponding biochemical processes in the host organism. The TCR associates to pMHC with a rate k_{on}, forming the first bound state in the system (Figure 6b). In the bound state, the TCR–pMHC complex can sequentially phosphorylate with a rate k_p. This corresponds to transitions from the state n to $n + 1$: see Figure 6b. But the TCR can also dissociate from the complex with a rate k_{off}, and we assume here that it also includes a fast dephosphorylation so that binding of TCR to pMHC can only happen from the state $n = 0$ to the state $n = 1$. The main idea of this theoretical model is that the activation starts when the system reaches the stationary-state concentration of the final phosphorylated complexes ($n = N$). This is needed in order for the system to have a persistent and robust signal for activation.

It is convenient to adopt a single-molecule view of the process and analyze the dynamics of transitions between different states of the single TCR–pMHC complex.[76] For this purpose, one can define a function $P_n(t)$ as the probability to reach the state n at time t. Initially, at $t = 0$, the system starts in the unbounded state $n = 0$, that is, the receptor and the ligand are unbound from each other. These probabilities evolve with time as described by the following master equations,

$$\frac{dP_0(t)}{dt} = k_{off}\sum_{n=1}^{N} P_n(t) - k_{on}P_0(t), \tag{21}$$

for $n = 0$,

$$\frac{dP_1(t)}{dt} = k_{on}P_0(t) - \left(k_p + k_{off}\right)P_1(t), \tag{22}$$

for $n = 1$,

$$\frac{dP_n(t)}{dt} = k_pP_{n-1}(t) - \left(k_p + k_{off}\right)P_n(t), \tag{23}$$

for $1 < n < N$, and

$$\frac{dP_N(t)}{dt} = k_pP_{N-1}(t) - k_{off}P_N(t), \tag{24}$$

for $n = N$. Because we consider a single complex, there is an additional normalization condition for probabilities to be found at different states,

$$\sum_{n=0}^{N} P_n(t) = 1. \tag{25}$$

At large times, the system reaches the stationary state and the probability to be found in the final phosphorylation state N can be explicitly evaluated as:[76]

$$P_N = \frac{k_{\text{on}}}{(k_{\text{on}} + k_{\text{off}})} \left(\frac{k_p}{k_p + k_{\text{off}}} \right)^{N-1} \tag{26}$$

The physical meaning of this expression can be explained using the following arguments. The first factor, $\frac{k_{\text{on}}}{(k_{\text{on}}+k_{\text{off}})}$, gives the probability for the system to form the bound TCR–pMHC complex, while the second factor, $\left(\frac{k_p}{k_p+k_{\text{off}}}\right)^{N-1}$, gives the probability that the bound state is the final phosphorylation state after $N-1$ sequential phosphorylation events [each happening with the probability $\left(\frac{k_p}{k_p+k_{\text{off}}}\right)$].

This theoretical model argues that the immune system activation starts after reaching the fully phosphorylated state $n = N$, and for this reason the time to reach the steady-state level of this state is critical in discrimination between self-peptides and foreign peptides. Note that we already explored such time scales in the analysis of the formation of morphogen gradients (see Section 2). These are local relaxation times that can be easily estimated for the KPR model of immune system activation,[76] yielding

$$\tau_N = \frac{1}{k_{\text{on}} + k_{\text{off}}} + \frac{N-1}{k_p + k_{\text{off}}}. \tag{27}$$

This expression can be interpreted in the following way. The first term gives the time for the system to achieve the stationary conditions with respect to all bounded and unbounded conformational states. The second term provides the estimate to reach the final phosphorylation state $n = N$ starting from the first association state $n = 1$. This is because after any dissociation ($n \to 0$) the next binding event always leads to the state $n = 1$, from which $N-1$ irreversible steps are needed in order to be fully phosphorylated.

The KPR model proposes the following mechanism of discrimination between self-peptides and foreign peptides.[76] It is argued that for self-ligands the relaxation times before reaching the active state $n = N$ are rapid, and they are faster than a specific threshold time t_0, which is determined by the local biochemical conditions of the organism. At this situation the activation does not happen. However, the relaxation times for foreign ligands are longer ($\tau_N > t_0$), and the activation triggers the immune system. Experimental observations suggest that these threshold times vary for different organisms, but typically they are in the range between 1 and 5 s.[58,79,80]

The application of the discrete-state stochastic model of T cells activation for two different biological systems is presented in Figure 7. It shows the calculated relaxation times and different degrees of ligand potency (expressed as EC_{50}) for various peptides. The ligand potency parameter EC_{50} is a concentration of the peptide that stimulates the activation of T cells in 50% cases. This means that the large values of EC_{50} correspond to a weak immune response, while the small values of EC_{50} induce a strong response. Thus, the theoretical model predicts that self-peptides should have large EC_{50}, while the situation is opposite for foreign ligands where small EC_{50} values are expected. Figure 7 clearly shows a separation of experimental observations in two groups. For observations with relaxation times smaller than the threshold (5 s for the upper plot and 2 s for the lower plot in Figure 7), the probability of activating the immune system is low because of large EC_{50} values. These are self-peptides. For observations with relaxation times larger than the thresholds, the immune system will be activated since these are foreign peptides. Thus, the discrete-state stochastic model of T cells activation not only successfully explains experimental data, but it also provides the microscopic description for the processes that lead to the activation of immune system.

5 | CANCER INITIATION DYNAMICS

Our final example of application of stochastic kinetic models for uncovering the mechanisms of complex biological processes is related to investigations of cancer initiation dynamics.[37,81] Cancer remains one of the most serious health problems in our society.[82–84] It is a set of genetic diseases that result from accumulation of unfavorable mutations in the living organisms. While the overall biochemical picture of how cancer appears is more or less known, the molecular

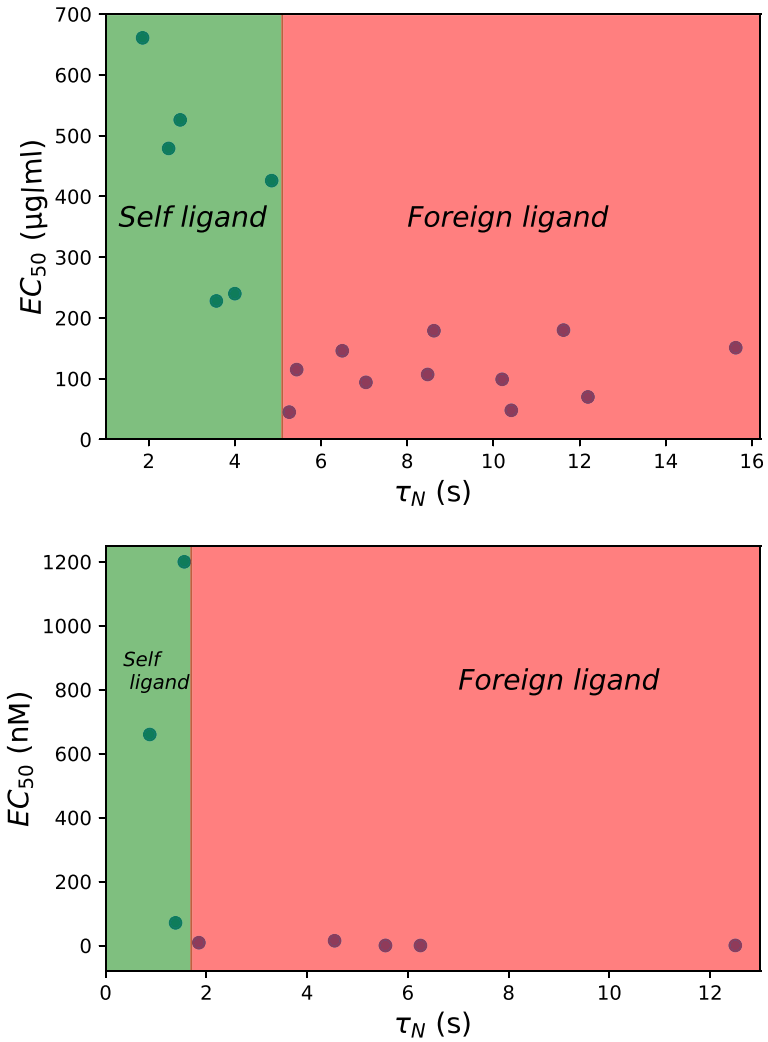

FIGURE 7 The relations between the relaxation times (τ_N) and the ligand potency (EC_{50}). The kinetic parameters k_{on} and k_{off} and the ligand potency EC_{50} to evaluate τ_N are taken from ref [79] (for the top plot), and from Ref. [58] (for the bottom plot). In calculations, $N = 6$ and $k_p = 0.1\ s^{-1}$ were utilized. The figures are reproduced with permission from Ref. [76]

details of the formation of tumors are still not fully understood. One of the most important directions to uncover the microscopic origin of the tumor formation is to analyze the dynamics of cancer initiation and progress.[84–86] The idea is that the dynamics reflects the underlying microscopic mechanisms. The stochastic model presented here addresses this challenge.

We start by considering an originally healthy tissue with N stem cells, as schematically shown in Figure 8. Stem cells are those that divide and produce new cells.[11] The replication process is known to be the main source of possible mutations because of potential chemical errors during the synthesis of new DNA molecules when these errors are not corrected on time by DNA repair mechanisms.[87,88] This is the main reason we concentrate only on stem cells. At some specific time point, which is set to zero, a mutation happens in one of the cells. Only those mutations that lead to the cancer, the so-called *driver* mutations, are considered.[89,90] All types of the tissue cells can divide, but with different rates. The normal stem cells divide with a rate b, while the mutated cells divide with a rate rb. The parameter r is known as a *fitness parameter*, and it specifies how the mutated cells differ from normal cells due to various physiological and biochemical changes. The situation when $r > 1$ describes the advantageous mutations (mutated cells divide faster than the normal cells), $r = 1$ corresponds to neutral mutations (the same division rates for mutated and normal cells), and for $r < 1$ the mutations are disadvantageous (mutated cells divide slower than the normal cells). It is believed that mutations that lead to the tumor formation are mostly advantageous.[8]

The appearance of few mutated cells in the tissue is not yet the sign of cancer. The organism operates normally, and it is in the so-called *homeostatic equilibrium*. The homeostasis has multiple features, but for this model it is important that in the healthy tissue the number of cells remains constant. Thus, if some cells divide then other cells must be

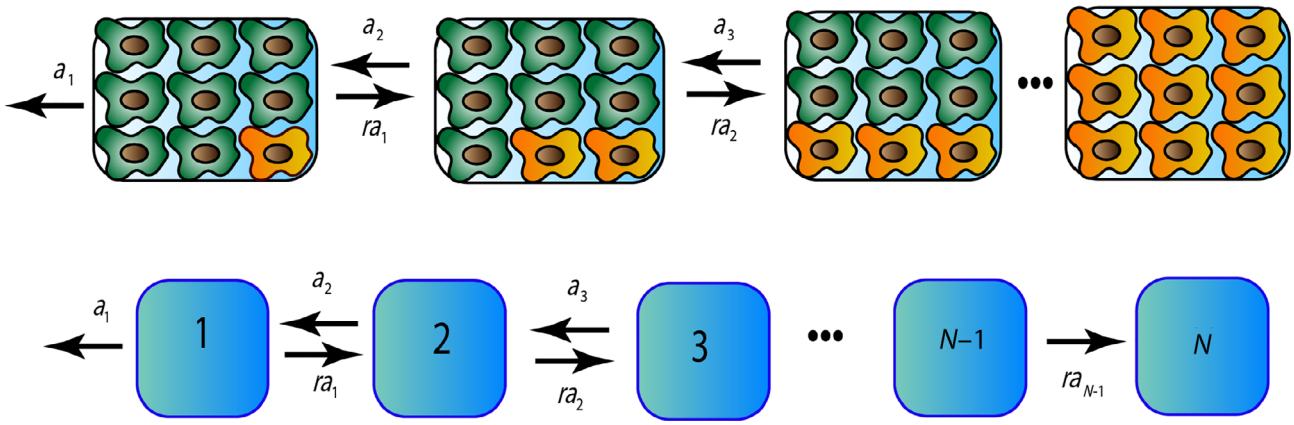

FIGURE 8 Top: A schematic view of a single mutation fixation process in the tissue compartment. Normal stem cells are green, while mutated cells are yellow. Bottom: Corresponding discrete-state stochastic model. The figure is reproduced with permission from Ref. [81]

removed to keep the total number cells in the tissue constant. The exact details of how it is happening are not known, but to imitate this dynamics it is assumed that the system follows a procedure known as a *Moran process*.[8,91,92] According to this approach, one of the N cells is randomly chosen for the division, and this increases the total number of cells in the tissue by one. But then immediately another randomly chosen cell from $N+1$ cells is removed, returning the number of cells in the tissue to the original count: see Figure 8. In addition, it is assumed that in the system only a single mutation might happen due to very low rates of mutations.[8,89] This means that the increase in the number of mutated cells in the tissue is taking place only due to random divisions of the mutated cells and random removals of the normal cells.

The state of the tissue at any moment can be characterized by a single parameter, the number of mutated cells n ($1 \le n \le N$).[81] This is because the total number of cells is fixed in the homeostasis. All changes in the system can be viewed as stochastic transitions between discrete states as visualized in Figure 8. In the sequence of states with different numbers of mutated cells (see Figure 8), there are only two possible outcomes. Due to random transitions, the mutation can be completely removed from the system, and this corresponds to $1 \to 0$ transition. But the other outcome is that the mutated cells fully occupy the tissue, that is, the system will reach the state $n = N$ (Figure 8). This is known as a mutation *fixation*, and the model assumes that this event marks the beginning of cancer.[8,81,84] After that, no normal cells are left in the tissue, and the system can break from the homeostasis.

Using the Moran processes rules,[8] the transition rates between the individual states of the system can be explicitly evaluated,[81]

$$a_n = b\frac{n(N-n)}{N+1}. \tag{28}$$

More specifically, the transition from the state n to $n+1$, which increases the number of mutated cells by one, is taking place with the rate ra_n. At the same time, the transition $n \to n-1$, which decreases the number of mutated cells, is taking place with the rate a_n.

In this model, it is postulated that the tumor appears as soon as the system reaches the state $n = N$ for the first time, starting at $t = 0$ in the state $n = 1$. This suggests that it is convenient to apply first-passage methods for this problem that were already utilized in some of the discussed above discrete-state stochastic kinetic models. For this purpose, one can define a first-passage probability density function $F_n(t)$ that corresponds to the probability of reaching the state N (fixation) for the first time at time t if at $t = 0$ the system started in the state n. The temporal evolution of these functions can be analyzed from a set of backward master equations,[55,56]

$$\frac{dF_n(t)}{dt} = ra_nF_{n+1}(t) + a_nF_{n-1}(t) - a_n(1+r)F_n(t), \tag{29}$$

for $1 < n < N$; and for $n = 1$ we have

$$\frac{dF_1(t)}{dt} = ra_1F_2(t) - a_1(1+r)F_1(t). \tag{30}$$

In addition, the boundary condition $F_N(t) = \delta(t)$ must be satisfied. The physical meaning of this condition is that the fixation process is immediately accomplished if the system starts from the state N.

While a full dynamic description can be obtained from the knowledge of the first-passage probability functions, to characterize these processes one could concentrate only on two important parameters. One of them is a fixation probability, $\pi_n \equiv \int_0^\infty F_n(t)dt$, and another one is a fixation time, $T_n \equiv \frac{\int_0^\infty tF_n(t)dt}{\int_0^\infty F_n(t)dt}$. The first parameter gives the overall probability to initiate the cancer, while the second parameter measures the average times before this might happen. Analytical calculations provide explicit expressions for both of these important characteristics.[36] For the fixation probability, it has been shown that,[8]

$$\pi_n = \frac{1-1/r^n}{1-1/r^N}. \tag{31}$$

For $r = 1$ (neutral mutations), the result simplifies into $\pi_n = n/N$, which means that the cancer initiation is more probable with the larger number of mutated cells in the initial state of the system. More importantly is to consider a start at the state $n = 1$, when the first mutation appears, and the fixation probability π_1 is presented in Figure 9a. As expected, increasing the fitness parameter r enhances the probability of tumor formation. This is clearly due to the fact that for $r > 1$ the mutated cells divide faster. Another observation is that for realistically large values of N the fixation probability is independent of the size of the tissue.

More interesting observations are found by analyzing the fixation times that are the mean times between the appearance of the first mutation and the state when all cells in the tissue are mutated. Analytical calculations yield,[81]

$$T_1 = \frac{N+1}{b}\sum_{n=1}^{N-1}\frac{1}{n(N-n)}\left(\frac{r^n-1}{r-1}\right)\left(\frac{r^{N-n}-1}{r^N-1}\right). \tag{32}$$

For neutral mutations in the tissues with large number of cells ($r = 1$ and $N \to \infty$), the expression simplifies into

$$T_1 \simeq N/b. \tag{33}$$

More generally, for large N the equation for the mean fixation times can be rewritten as

$$T_1 = \frac{1}{b}\frac{1}{r\left(1-\frac{1}{r^N}\right)}\left[\frac{\mathrm{Ei}(-\ln r)}{\ln r}\left(1-\frac{1}{r}\right)+\frac{2}{\ln r}(\gamma+\ln[N\ln r])\right], \tag{34}$$

where $\mathrm{Ei}(x)$ is the exponential integral defined as $\mathrm{Ei}(x) \equiv -\int_{-x}^{\infty}\frac{e^{-z}}{z}dz$, and γ is the Euler-Mascheroni constant.

Calculated average times before the cancer initiation are presented in Figure 9b that shows some surprising observations. While increasing the fitness parameter r should accelerate the appearance of the tumors, and this is supported by the results in Figure 9b, the slowest cancer initiation dynamics is found for neutral mutations $r = 1$. This situation is similar to the dynamics of bacterial clearance that we already considered before. For $r = 1$ the system behaves similarly to the unbiased random walk along the lattice of sites in Figure 8 that leads to the slow dynamics. The unexpected result is that even for $r < 1$ the tumor formation might be fast, which contradicts to naive expectations: in this case the normal cells divide faster than the mutated cells. One could explain this by noticing the definition of the mean fixation time. It is a conditional time to achieve the state $n = N$ given that the system can reach it. For disadvantageous mutations ($r < 1$), the fixation probability is low since the system dynamics is biased in the direction of eliminating the mutations (to the left in Figure 8). But those rare successful fixation events must happen fast because at every intermediate step the system can reverse the direction due to the bias against the fixation. Interestingly, these results support some of the controversial theoretical arguments that only neutral mutations are possible in biological systems since the evolution might already explored the faster advantageous and disadvantageous mutations.[8]

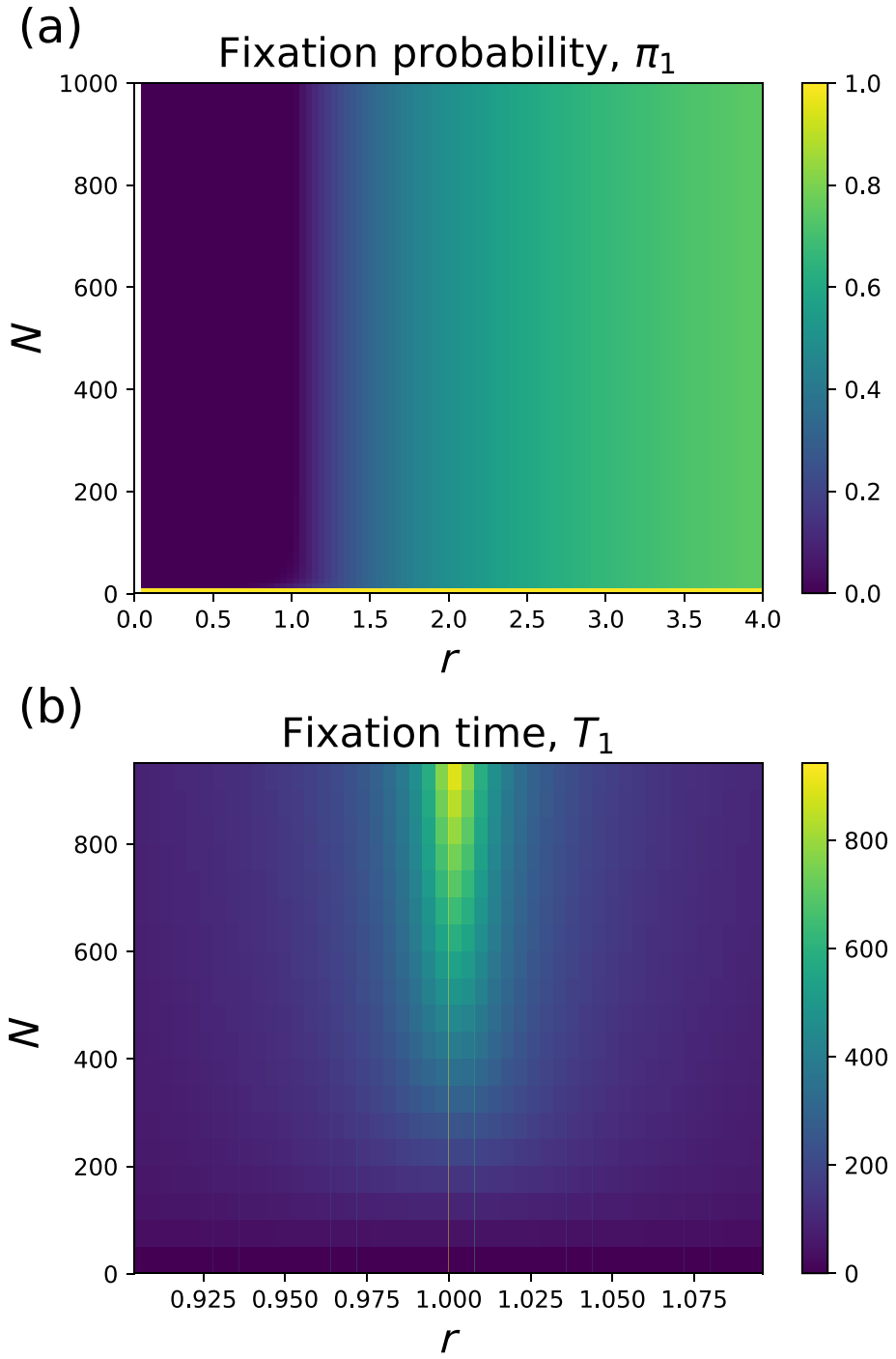

FIGURE 9 Heat maps for (a) fixation probability π_1 and (b) fixation time τ_1 (normalized with respect to the normal stem cell replication time, i.e., $b = 1$) as a function parameters r and N. the figures are reproduced with permission from Ref. [81]

This discrete-state stochastic model for cancer initiation has been applied to analyze the data from 28 types of cancer.[81] Explicit estimates of the average times before the formation of different types of tumors have been obtained. But the most important result from this theoretical approach is the analysis of correlations between the cancer lifetime risks and mean cancer initiation times. The cancer lifetime risk, which is defined as the probability to get cancer or to die from cancer during the human lifetime, is widely used in forecasting the chances of getting the cancers. It implicitly assumes that the more probable cancers (higher lifetime risks) will happen faster. The discrete-state stochastic model is capable to estimate the initiation times from real data. Surprisingly, the analysis shows that there is no correlation between the cancer lifetime risks and mean times to get the tumor. One can see this from Figure 10. Statistical analysis

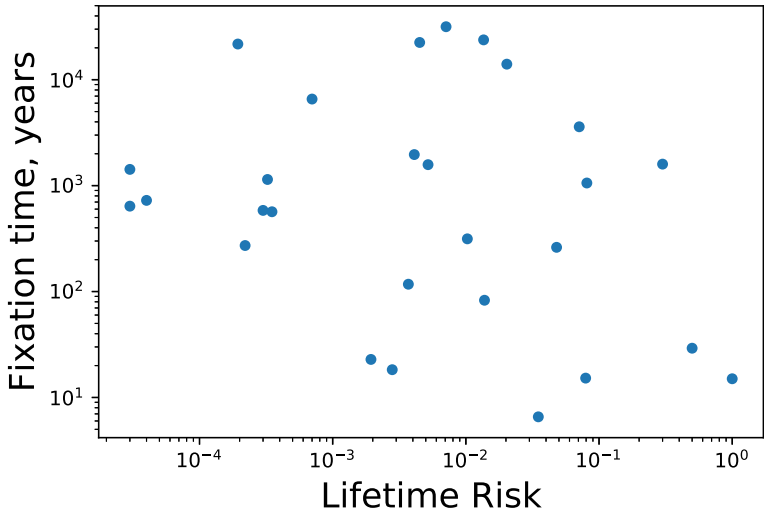

FIGURE 10 Calculated fixation times as a function of measured lifetime risks for different types of cancer. The figure is reproduced with permission from Ref. [81]

of this graph gives a Spearman's correlation coefficient −0.2 between the cancer lifetime risks and the fixation times, magnitude of which is significantly smaller than the value −1 expected for the perfect correlation. Another statistical test, the *P*-value analysis, also indicates the lack of correlations between two dynamic properties of cancer initiation.

While the lack of correlations between the cancer lifetime risks and cancer initiation times is clearly unexpected, one should notice that similar situations have been encountered in other complex systems. More specifically, this is frequently observed in chemical reactions. While the probability for reaction to happen is determined by the free energy difference between the products and reagents, the actual time for reaction to occur is given by the height of the activation energy barrier.[1] These two energy scales are not always correlating in chemical processes. The fact that similar events are taking place in the cancer initiation dynamics possibly suggests a similar microscopic mechanism with an effective barrier in the mutation fixation process. It could be that not the fixation parameter r specifies how fast the tumor will form but the barrier for the dynamic transitions on the pathway to the mutation fixation.

6 | CONCLUSION

We presented several stochastic kinetic models and their applications for studies of various complex biological processes. While each of the model was specifically tailored for the given problem, there are some common features that allow us to understand the success of this theoretical approach. In all systems, the underlying complex processes were mapped into the network of stochastic transitions between specific discrete states. This procedure lead to explicit analytical description of dynamic processes that also clarified many aspects of the molecular mechanisms. The advantage of this theoretical method is that it can be extended by taking into account larger and more complex networks of states that might better reflect the properties of the systems. Theoretical predictions are also easy to apply for the analysis of available experimental data and for predicting new observations. Another advantage is that one can utilize the analogies with already well-studied systems to draw conclusions and propose mechanisms for these biological processes. It seems that the stochastic kinetic method, together with more microscopic biochemical approaches and with experimental support, might be a powerful tool in uncovering the mysteries of natural phenomena.

ACKNOWLEDGMENTS

The work was supported by the Welch Foundation (C-1559), by the NSF (CHE-1953453 and MCB-1941106), and by the Center for Theoretical Biological Physics sponsored by the NSF (PHY-2019745).

CONFLICT OF INTEREST

The authors declare no conflict of interest.

AUTHOR CONTRIBUTIONS

Hamid D. Teimouri: Conceptualization (supporting); data curation (supporting); formal analysis (supporting); investigation (equal); methodology (equal); software (lead); writing – original draft (lead); writing – review and editing (equal). **Anatoly Kolomeisky:** Conceptualization (lead); data curation (lead); formal analysis (equal); funding acquisition (lead); investigation (equal); methodology (equal); project administration (lead); resources (equal); supervision (lead); writing – review and editing (equal).

DATA AVAILABILITY STATEMENT

Data sharing is not applicable to this article as no new data were created or analyzed in this study.

ORCID

Hamid Teimouri https://orcid.org/0000-0002-3319-1187
Anatoly B. Kolomeisky https://orcid.org/0000-0001-5677-6690

RELATED WIRES ARTICLES

Bridging chromatin structure and function over a range of experimental spatial and temporal scales by molecular modeling

REFERENCES

1. Houston PL. Chemical kinetics and reaction dynamics. Chelmsford, MA: Courier Corporation; 2012.
2. Nelson DL, Lehninger AL, Cox MM. Lehninger principles of biochemistry. New York, NY: Macmillan; 2008.
3. Irurzun-Arana I, Rackauckas C, McDonald TO, Trocóniz IF. Beyond deterministic models in drug discovery and development. Trends Pharmacol Sci. 2020;41:882–95.
4. Resat H, Petzold L, Pettigrew MF. Kinetic modeling of biological systems. Comput Syst Biol. 2009;541:311–35.
5. Beard DA, Qian H. Chemical biophysics: quantitative analysis of cellular systems. Vol 126. Cambridge: Cambridge University Press; 2008.
6. Makarov DE. Single molecule science: physical principles and models. Boca Raton, FL: CRC Press; 2015.
7. Bressloff PC, Newby JM. Stochastic models of intracellular transport. Rev Mod Phys. 2013;85(1):135–96.
8. Nowak MA. Evolutionary dynamics: exploring the equations of life. Cambridge, MA: Harvard University Press; 2006.
9. Arias AM, Stewart A. Molecular principles of animal development. Oxford, England: Oxford University Press; 2002.
10. Wolpert L, Tickle C, Arias AM. Principles of development. Oxford, England: Oxford University Press; 2015.
11. Lodish H, Berk A, Kaiser CA, Kaiser C, Krieger M, Scott MP, et al. Molecular cell biology. New York, NY: Macmillan; 2008.
12. Crick F. Diffusion in embryogenesis. Nature. 1970;225(5231):420–2.
13. Porcher A, Dostatni N. The bicoid morphogen system. Curr Biol. 2010;20(5):R249–54.
14. Lander AD. Morpheus unbound: reimagining the morphogen gradient. Cell. 2007;128(2):245–56.
15. Rogers KW, Schier AF. Morphogen gradients: from generation to interpretation. Annu Rev Cell Dev Biol. 2011;27:377–407.
16. Teimouri H, Kolomeisky AB. Mechanisms of the formation of biological signaling profiles. J Phys A: Math Theor. 2016;49(48):483001.
17. Kolomeisky AB. Formation of a morphogen gradient: acceleration by degradation. J Phys Chem Lett. 2011;2(13):1502–5.
18. Berezhkovskii AM, Shvartsman SY. Kinetics of receptor occupancy during morphogen gradient formation. J Chem Phys. 2013;138(24):244105.
19. Mogilner A, Odde D. Modeling cellular processes in 3D. Trends Cell Biol. 2011;21(12):692–700.
20. Little SC, Tkačik G, Kneeland TB, Wieschaus EF, Gregor T. The formation of the Bicoid morphogen gradient requires protein movement from anteriorly localized mRNA. PLoS Biol. 2011;9(3):e1000596.
21. Dalessi S, Neves A, Bergmann S. Modeling morphogen gradient formation from arbitrary realistically shaped sources. J Theor Biol. 2012;294:130–8.
22. Berezhkovskii AM, Sample C, Shvartsman SY. Formation of morphogen gradients: local accumulation time. Phys Rev E. 2011;83(5):051906.
23. Gordon PV, Muratov CB, Shvartsman SY. Local accumulation times for source, diffusion, and degradation models in two and three dimensions. J Chem Phys. 2013;138(10):03B607.
24. Briscoe J, Small S. Morphogen rules: design principles of gradient-mediated embryo patterning. Development. 2015;142(23):3996–4009.
25. Wartlick O, Kicheva A, Gonzalez-Gaitan M. Morphogen gradient formation. Cold Spring Harb Perspect Biol. 2009;1(3):a001255.
26. Teimouri H, Kolomeisky AB. The role of source delocalization in the development of morphogen gradients. Phys Biol. 2015;12(2):026006.
27. Teimouri H, Bozorgui B, Kolomeisky AB. Development of morphogen gradients with spatially varying degradation rates. J Phys Chem B. 2016;120(10):2745–50.
28. Gregor T, Wieschaus EF, McGregor AP, Bialek W, Tank DW. Stability and nuclear dynamics of the bicoid morphogen gradient. Cell. 2007;130(1):141–52.

29. Yu SR, Burkhardt M, Nowak M, Ries J, Petrášek Z, Scholpp S, et al. Fgf8 morphogen gradient forms by a source-sink mechanism with freely diffusing molecules. Nature. 2009;461(7263):533–6.
30. Drocco JA, Grimm O, Tank DW, Wieschaus E. Measurement and perturbation of morphogen lifetime: effects on gradient shape. Biophys J. 2011;101(8):1807–15.
31. Kicheva A, Pantazis P, Bollenbach T, Kalaidzidis Y, Bittig T, Jülicher F, et al. Kinetics of morphogen gradient formation. Science. 2007; 315(5811):521–5.
32. Berezhkovskii AM, Sample C, Shvartsman SY. How long does it take to establish a morphogen gradient. Biophys J. 2010;99(8):L59–61.
33. Hecht I, Rappel WJ, Levine H. Determining the scale of the Bicoid morphogen gradient. Proc Natl Acad Sci. 2009;106(6):1710–5.
34. Berezhkovskii AM, Shvartsman SY. Physical interpretation of mean local accumulation time of morphogen gradient formation. J Chem Phys. 2011;135(15):10B618.
35. Castle BT, Howard SA, Odde DJ. Assessment of transport mechanisms underlying the bicoid morphogen gradient. Cell Mol Bioeng. 2011;4(1):116–21.
36. Teimouri H, Kolomeisky AB. Theoretical investigation of stochastic clearance of bacteria: first-passage analysis. J R Soc Interface. 2019; 16(152):20180765.
37. Teimouri H, Kolomeisky AB. Temporal order of mutations influences cancer initiation dynamics. Phys Biol. 2021;18:056002.
38. Reller LB, Weinstein M, Jorgensen JH, Ferraro MJ. Antimicrobial susceptibility testing: a review of general principles and contemporary practices. Clin Infect Dis. 2009;49(11):1749–55.
39. Allen R, Waclaw B. Antibiotic resistance: a physicist's view. Phys Biol. 2016;13(4):045001.
40. Nielsen EI, Cars O, Friberg LE. Predicting in vitro antibacterial efficacy across experimental designs with a semi-mechanistic PKPD model. Antimicrob Agents Chemother. 2011;55:1571–9.
41. Ferro BE, van Ingen J, Wattenberg M, van Soolingen D, Mouton JW. Time–kill kinetics of antibiotics active against rapidly growing mycobacteria. J Antimicrob Chemother. 2014;70(3):811–7.
42. Regoes RR, Wiuff C, Zappala RM, Garner KN, Baquero F, Levin BR. Pharmacodynamic functions: a multiparameter approach to the design of antibiotic treatment regimens. Antimicrob Agents Chemother. 2004;48(10):3670–6.
43. Czock D, Markert C, Hartman B, Keller F. Pharmacokinetics and pharmacodynamics of antimicrobial drugs. Expert Opin Drug Metab Toxicol. 2009;5(5):475–87.
44. Falagas ME, Tansarli GS, Rafailidis PI, Kapaskelis A, Vardakas KZ. Impact of antibiotic MIC on infection outcome in patients with susceptible gram-negative bacteria: a systematic review and meta-analysis. Antimicrob Agents Chemother. 2012;56(8):4214–22.
45. Jones RM, Nicas M, Hubbard AE, Reingold AL. The infectious dose of Coxiella burnetii (Q fever). Appl Biosaf. 2006;11(1):32–41.
46. Heppell CW, Egan JR, Hall I. A human time dose response model for Q fever. Epidemics. 2017;21:30–8.
47. Hara-Kudo Y, Takatori K. Contamination level and ingestion dose of foodborne pathogens associated with infections. Epidemiol Infect. 2011;139(10):1505–10.
48. Gullberg E, Cao S, Berg OG, Ilbäck C, Sandegren L, Hughes D, et al. Selection of resistant bacteria at very low antibiotic concentrations. PLoS Pathog. 2011;7(7):e1002158.
49. Kohanski MA, DePristo MA, Collins JJ. Sublethal antibiotic treatment leads to multidrug resistance via radical-induced mutagenesis. Mol Cell. 2010;37(3):311–20.
50. Dagan R, Klugman KP, Craig WA, Baquero F. Evidence to support the rationale that bacterial eradication in respiratory tract infection is an important aim of antimicrobial therapy. J Antimicrob Chemother. 2001;47(2):129–40.
51. Tomita T, Fukuda Y, Tamura K, Tanaka J, Hida N, Kosaka T, et al. Successful eradication of helicobacter pylori prevents relapse of peptic ulcer disease. Aliment Pharmacol Ther. 2002;16:204–9.
52. Wilson R, Sethi S, Anzueto A, Miravitlles M. Antibiotics for treatment and prevention of exacerbations of chronic obstructive pulmonary disease. J Infect. 2013;67(6):497–515.
53. Coates J, Park BR, Le D, Şimşek E, Chaudhry W, Kim M. Antibiotic-induced population fluctuations and stochastic clearance of bacteria. Elife. 2018;7:e32976.
54. Greulich P, Scott M, Evans MR, Allen RJ. Growth-dependent bacterial susceptibility to ribosome-targeting antibiotics. Mol Syst Biol. 2015;11(3):796.
55. Redner S. A guide to first-passage processes. Cambridge, England: Cambridge University Press; 2001.
56. Kolomeisky AB. Motor proteins and molecular motors. Boca Raton, FL: CRC Press; 2015.
57. Brauner A, Fridman O, Gefen O, Balaban NQ. Distinguishing between resistance, tolerance and persistence to antibiotic treatment. Nat Rev Microbiol. 2016;14(5):320–30.
58. Govern CC, Paczosa MK, Chakraborty AK, Huseby ES. Fast on-rates allow short dwell time ligands to activate T cells. Proc Natl Acad Sci. 2010;107(19):8724–9.
59. Lever M, Maini PK, Van Der Merwe PA, Dushek O. Phenotypic models of T cell activation. Nat Rev Immunol. 2014;14(9):619–29.
60. Chakraborty AK, Weiss A. Insights into the initiation of TCR signaling. Nat Immunol. 2014;15(9):798–807.
61. François P, Altan-Bonnet G. The case for absolute ligand discrimination: modeling information processing and decision by immune T cells. J Stat Phys. 2016;162(5):1130–52.
62. Feinerman O, Germain RN, Altan-Bonnet G. Quantitative challenges in understanding ligand discrimination by $\alpha\beta$ T cells. Mol Immunol. 2008;45(3):619–31.

63. Fernandes RA, Ganzinger KA, Tzou JC, Jönsson P, Lee SF, Palayret M, et al. A cell topography-based mechanism for ligand discrimination by the T cell receptor. Proc Natl Acad Sci U S A. 2019;116(28):14002–10.
64. François P, Voisinne G, Siggia ED, Altan-Bonnet G, Vergassola M. Phenotypic model for early T-cell activation displaying sensitivity, specificity, and antagonism. Proc Natl Acad Sci. 2013;110(10):E888–97.
65. Altan-Bonnet G, Germain RN. Modeling T cell antigen discrimination based on feedback control of digital ERK responses. PLoS Biol. 2005;3(11):e356.
66. Kersh GJ, Allen PM. Essential flexibility in the T-cell recognition of antigen. Nature. 1996;380(6574):495–8.
67. van der Merwe PA. The TCR triggering puzzle. Immunity. 2001;14(6):665–8.
68. Gaud G, Lesourne R, Love PE. Regulatory mechanisms in T cell receptor signalling. Nat Rev Immunol. 2018;18(8):485–97.
69. Smith-Garvin JE, Koretzky GA, Jordan MS. T cell activation. Annu Rev Immunol. 2009;27:591–619.
70. Cohen CJ, Sarig O, Yamano Y, Tomaru U, Jacobson S, Reiter Y. Direct phenotypic analysis of human MHC class I antigen presentation: visualization, quantitation, and in situ detection of human viral epitopes using peptide-specific, MHC-restricted human recombinant antibodies. J Immunol. 2003;170(8):4349–61.
71. Unternaehrer JJ, Chow A, Pypaert M, Inaba K, Mellman I. The tetraspanin CD9 mediates lateral association of MHC class II molecules on the dendritic cell surface. Proc Natl Acad Sci. 2007;104(1):234–9.
72. Irvine DJ, Purbhoo MA, Krogsgaard M, Davis MM. Direct observation of ligand recognition by T cells. Nature. 2002;419(6909):845–9.
73. Limozin L, Bridge M, Bongrand P, Dushek O, van der Merwe PA, Robert P. TCR–pMHC kinetics under force in a cell-free system show no intrinsic catch bond, but a minimal encounter duration before binding. Proc Natl Acad Sci. 2019;116(34):16943–8.
74. Yousefi OS, Günther M, Hörner M, Chalupsky J, Wess M, Brandl SM, et al. Optogenetic control shows that kinetic proofreading regulates the activity of the T cell receptor. Elife. 2019;8:e42475.
75. Tischer DK, Weiner OD. Light-based tuning of ligand half-life supports kinetic proofreading model of T cell signaling. Elife. 2019;8:e42498.
76. Teimouri H, Kolomeisky AB. Relaxation times of ligand-receptor complex formation control T cell activation. Biophys J. 2020;119(1):182–9.
77. Hopfield JJ. Kinetic proofreading: a new mechanism for reducing errors in biosynthetic processes requiring high specificity. Proc Natl Acad Sci. 1974;71(10):4135–9.
78. McKeithan TW. Kinetic proofreading in T-cell receptor signal transduction. Proc Natl Acad Sci. 1995;92(11):5042–6.
79. Aleksic M, Dushek O, Zhang H, Shenderov E, Chen JL, Cerundolo V, et al. Dependence of T cell antigen recognition on T cell receptor-peptide MHC confinement time. Immunity. 2010;32(2):163–74.
80. Stone JD, Chervin AS, Kranz DM. T-cell receptor binding affinities and kinetics: impact on T-cell activity and specificity. Immunology. 2009;126(2):165–76.
81. Teimouri H, Kochugaeva MP, Kolomeisky AB. Elucidating the correlations between cancer initiation times and lifetime cancer risks. Sci Rep. 2019;9(1):1–8.
82. Hanahan D, Weinberg RA. Hallmarks of cancer: the next generation. Cell. 2011;144(5):646–74.
83. Frank SA. Dynamics of cancer: incidence, inheritance, and evolution. Vol 1. Princeton, NJ: Princeton University Press; 2007.
84. Dominik W, Natalia K. Dynamics of cancer: mathematical foundations of oncology. Singapore: World Scientific; 2014.
85. Lytle NK, Barber AG, Reya T. Stem cell fate in cancer growth, progression and therapy resistance. Nat Rev Cancer. 2018;18:669–80.
86. Foo J, Leder K, Michor F. Stochastic dynamics of cancer initiation. Phys Biol. 2011;8(1):015002.
87. Tomasetti C, Vogelstein B. Variation in cancer risk among tissues can be explained by the number of stem cell divisions. Science. 2015;347(6217):78–81.
88. Tomasetti C, Li L, Vogelstein B. Stem cell divisions, somatic mutations, cancer etiology, and cancer prevention. Science. 2017;355(6331):1330–4.
89. Pon JR, Marra MA. Driver and passenger mutations in cancer. Annu Rev Pathol: Mech Dis. 2015;10:25–50.
90. McFarland CD, Mirny LA, Korolev KS. Tug-of-war between driver and passenger mutations in cancer and other adaptive processes. Proc Natl Acad Sci. 2014;111(42):15138–43.
91. Moran PAP. The statistical processes of evolutionary theory. Oxford: Claderon Press; 1962.
92. Moran PAP. Random processes in genetics. Mathematical proceedings of the Cambridge philosophical society. Volume 54. Cambridge, England: Cambridge University Press; 1958. p. 60–71.

How to cite this article: Teimouri H, Kolomeisky AB. Power of stochastic kinetic models: From biological signaling and antibiotic activities to T cell activation and cancer initiation dynamics. WIREs Comput Mol Sci. 2022. e1612. https://doi.org/10.1002/wcms.1612